A Vibrating Plate Fabricated by the Methods of Microelectromechanical Systems (MEMS) for the Simultaneous Measurement of Density and Viscosity: Results for Argon at Temperatures Between 323 and 423 K at Pressures up to 68 MPa[1]

A. R. H. Goodwin,[2,3,4] **A. D. Fitt,**[5] **K. A. Ronaldson,**[5] **and W. A. Wakeham**[6]

In the petroleum industry, measurements of the density and viscosity of petroleum reservoir fluids are required to determine the value of the produced fluid and the production strategy. Measurements of the density and viscosity of petroleum fluids require a transducer that can operate at reservoir conditions, and results with an uncertainty of about ±1% in density and ±10% in viscosity are needed to guide value and exploitation calculations with sufficient rigor. Necessarily, these specifications place robustness as a superior priority to accuracy for the design. A vibrating plate, with dimensions of the order of 1 mm and a mass of about 0.12 mg, clamped along one edge, has been fabricated, with the methods of Microelectromechanical (MEMS) technology, to provide measurements of both density and viscosity of fluids in which it is immersed. The resonance frequency (at pressure $p = 0$ is about 12 kHz) and quality factor (at $p = 0$ is about 2 800) of the first order bending (flexural) mode of the plate are combined with semi-empirical working equations, coefficients obtained by calibration, and the mechanical properties of the plate to provide the density and viscosity of the fluid into which

---

[2] Schlumberger-Doll Research, 36 Old Quarry Road, Ridgefield, Connecticut 06877, U.S.A.
[3] Present address: Schlumberger, 125 Industrial Blvd., Sugar Land, Texas 77478, U.S.A.
[4] To whom correspondence should be addressed. E-mail: Agoodwin@slb.com
[5] School of Mathematics, University of Southampton, Highfield, Southampton SO17 1BJ, United Kingdom.
[6] School of Engineering Sciences, University of Southampton, Highfield, Southampton SO17 1BJ, United Kingdom.

it is immersed. When the device was surrounded by argon at temperatures between 348 and 423 K and at pressures between 20 and 68 MPa, the density and viscosity were determined with an expanded ($k = 2$) uncertainty, including the calibration, of about $\pm 0.35\%$ and $\pm 3\%$, respectively. These results, when compared with accepted correlations for argon reported in the literature, were found to lie within $\pm 0.8\%$ for density and less than $\pm 5\%$ for viscosity of literature values, which are within a reasonable multiple of the relative combined expanded ($k = 2$) uncertainty.

1. INTRODUCTION

The evaluation of the economic viability of a hydrocarbon-bearing formation requires measurements of many physical properties. In particular, the thermophysical properties of hydrocarbon reservoir fluids are required to determine flow in porous media and design completion, separation, treating, and metering systems. The financial analysis that provides the potential for commercial benefit from exploitation of naturally occurring hydrocarbon resources is determined from knowledge of the reservoir permeability, size, shape, and compartmentalization and the fluid thermophysical properties. The uncertainties in viscosity, density, and phase behavior of the petroleum fluid impact the financial analysis.

The reservoir often comprises a group of fluid bearing layers separated by impermeable shale. The physical properties of the fluids can be determined from measurements performed on a sub-sample of an aliquot extracted from each layer. Often the extraction is performed after the borehole has been drilled but before the production system, consisting of metal tubes surrounded by cement, is installed. From these down-hole samples, all physical properties of the fluid can be determined in a laboratory at reservoir temperature along with the variations with temperature and pressure that will be experienced throughout the production system. Typically, reservoir temperatures are less than 473 K at pressures below 200 MPa. These measurements are combined with knowledge of the permeability of the reservoir and the reservoir size, shape and compartmentalization to perform analyses concerning the development of that petroleum reservoir. From this list, the thermophysical properties and their uncertainties are usually considered to be lower in priority than the other items in the financial analysis. However, uncertainties in the thermophysical properties, particularly for retrograde condensates, that arise from the operating conditions (reservoir conditions as well as at temperatures and pressures experienced throughout the production system) and sampling techniques

can be significant and may be reduced by direct measurement. In general, measurements of density and viscosity with uncertainties of about ±1 and ±10%, respectively, are considered adequate to guide value and exploitation calculations with sufficient rigor. Thus, methods that can provide *in situ* measurements of fluid density and viscosity with these uncertainties at the reservoir temperature are desirable because they reduce both the time required for analysis and systematic errors that might arise from variations in chemical composition caused by transferring the fluids from one container to another and subsequent transportation.

Of the numerous methods that have been reported to measure density [1–5] and viscosity [6–11], the most relevant to the instrument discussed here are those that utilize a vibrating object of defined geometry and are fabricated by the methods of microelectromechanical systems (MEMS) technology. To our knowledge, the instrument reported by Woodward [12], although not a MEMS device, is the earliest example of a vibrating object that is conceptually similar to the device described here. In Ref. [12], a 0.25 mm thick steel disk with a diameter of about 5 mm was connected via a narrow neck to a clamp. The disk was forced to vibrate, and measurements of the resonance were used to determine the product of density and viscosity. There are many articles describing transducers for the measurement of density and viscosity fabricated by the methods of MEMS in the archival literature, and here we give four examples. Andrews and Harris [13] have described a device with two parallel plates, each supported by beams, that are oscillated normal to each other to determine the viscosity of gases while Martin et al. [14] presented a flexural plate wave resonator, fabricated on a silicon nitride membrane, to determine density. There are also fluid-filled vibrating U-tube densimeters fabricated with MEMS albeit with a square rather than the traditional circular cross section [15–17]. In addition to these devices, there are numerous applications of cantilever beams (developed from the devices used in atomic force microscopy [18]) to the measurement of density and viscosity [19–28]. The width and length of cantilevers vary from about 2 to 200 μm with a thickness of the order of 1 μm [29].

To develop a method for *in situ* and simultaneous measurements of density and viscosity, we have chosen to construct a vibrating object. The geometry of the device was constrained by the requirements to derive working equations for a well-defined shape of known dimensions and, when fabricated by the methods of MEMS, these constraints necessarily precluded the use of curved surfaces. In particular, we have developed a transducer, shown in Fig. 1, which is similar to a cantilever in that it is a rectangular plate connected to a support along one edge. However, the device described here has a width of about 2 mm, a length of about
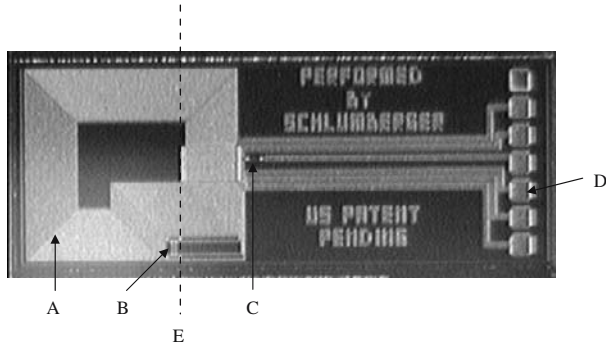
Fig. 1. Photograph of the top surface of the MEMS device showing the aluminum coil A, Wheatstone bridge B, boron-doped polycrystalline silicon resistor C that acted as thermometer, and wire-bond pads D. The $\approx 22.25\,\mu$m thick plate is to the left of dashed line E, and to the right of the dashed line the MEMS has an additional $\approx 350\,\mu$m thick mono-crystalline silicon.

1.5 mm, and a thickness of about $20\,\mu$m. The density and viscosity of the fluid in which the plate is immersed have been determined from measurements of the first, non-zero frequency eigenmode, which is a symmetrical bending mode with flexural motion. The design of the edge-supported vibrating plate densimeter/viscometer described here, and shown in Fig. 1, is based on a magnetic field sensor reported by Donzier et al. [30] and also fabricated by the methods of MEMS. The object developed for this work was fabricated from mono-crystalline silicon, a mechanically stable material, by addition of layers to produce a means of exciting and detecting the motion of the plate near resonance. This MEMS sensor utilizes silicon-on-insulator (SOI) wafers, photolithography (as used in integrated circuit fabrication), and deep reactive ion etching for the micro-machining.

When the MEMS fabricated transducer, illustrated in Fig. 1, is placed in a fluid, its resonance frequency f and quality factor $Q(= f/2g)$ decrease with increasing density and viscosity, respectively. The parameter g is the resonance line width between f and a frequency at which the measured amplitude is $2^{-1/2}$ times the maximum value at f. The general effect of the fluid on the plate can be understood by two straightforward approximations. First, the resonant frequency decreases with increasing density because of added mass. Second, Q decreases as the viscosity increases resulting mostly from the shearing motion at the tip of the plate. The methods of MEMS technology have provided a means of constructing a densimeter that has a resonance frequency sensitive to the added mass

of fluid in which it is immersed. This arises because the plate has a large surface-to-volume ratio and a mass of about 0.12 mg. The plate mass is equal to the mass of argon at $T = 323$ K and $p = 7$ MPa contained in about 70 viscous skin depths $[\delta = \{\eta/(\rho\pi f)\}^{1/2}$ each of about 3.3×10^{-6} m where ρ is the density and η the fluid viscosity] around the plate when the plate resonates at a frequency of about 7.6 kHz; at $T = 323$ K and $p = 68$ MPa, $\delta = 2.5 \times 10^{-6}$ m.

Typically, reservoir gases have densities in the range 100–500 kg·m^{-3} and viscosities between 0.01 and 0.1 mPa·s. Fluids that include at least these ranges of density and viscosity are required for the laboratory evaluation of proposed measurement techniques and calibration of other viscometers and densimeters as a function of both temperature and pressure [31–33]. In this article, we are concerned solely with argon at densities between 79 and 767 kg·m^{-3} and viscosities in the range of 26–57 μPa·s. In another article [34] we reported measurements when a similar MEMS densimeter/viscometer was exposed to liquid methylbenzene and octane with densities between 619 and 890 kg·m^{-3} and viscosities in the range of 0.205–0.711 mPa·s. For this work and that described in Ref. [34], the fluids are Newtonian so that their viscosity is independent of the rate of shear. However, non-Newtonian fluids are also encountered in the production of petroleum, as for example in the case of a drilling lubricant that contains sodium bentonite which has been added to increase the density. A transducer suitable for operation in both Newtonian and non-Newtonian fluids is the subject of another article [35]; we anticipate for the Newtonian fluid case the device discussed here will provide the product of density and viscosity.

2. WORKING EQUATIONS

The model, presented in detail elsewhere [34], describes the plate oscillating in an inviscid fluid decoupling the effect of viscosity and density so that the density is determined solely from the resonance frequency, and an independent equation is used to determine the viscosity. The plate is modeled as a beam supported at one end, $z = 0$ and $y = 0$, as illustrated schematically in Fig. 2. If we assume that longitudinal strain varies linearly across the plate's depth and the bending moment at any cross section is proportional to a local radius of curvature and we consider only the first eigenmode (1,0) so terms containing derivatives in x can be eliminated, then the partial differential equation for the force applied normal to the plate F can be estimated from the Bernoulli–Euler bending theory of thin plates. In this analysis, we have assumed the fluid is inviscid and incompressible and the boundary conditions are pinned or simply-supported.
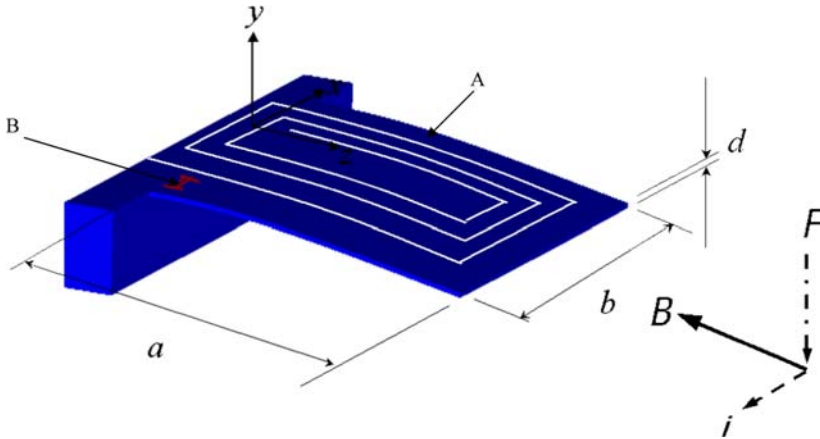
Fig. 2. Isometric projection of a MEMS plate of length a, width b, and thickness d illustrating the relative positions of the applied magnetic flux B, the direction of the current i through the coil A, and the resulting force F creating a motion in the y plane that is detected by the Wheatstone bridge B.

This implies at the supported end ($z=0$) the oscillating plate has neither deflection nor bending so that the displacement q satisfies $q=\partial^2 q/\partial z^2=0$ and at the free end of the plate ($z=a$) (the furthest distance from the support) there is neither bending nor shear force so $\partial^2 q/\partial z^2=\partial^3 q/\partial z^3=0$. When we assume there is no force acting on the plate (i.e., in vacuo) and the plate oscillates with harmonic motion, the eigenvalues, υ_n satisfy $\tan(a\upsilon_n)=\tanh(a\upsilon_n)$ (so that the first eigenvalue $\upsilon_1=3.926602312$) provided that $48\rho_s\pi^2 f^2 a^4(1-\sigma^2)=Ed^2\upsilon_n^4$ (see below for the definition of the parameters). The MEMS plate is about 2×10^{-5} m thick, assuming uniformity along the length, and about 1.5×10^{-3} m long and thus satisfies the slender body criteria which can be applied to the oscillations of the plate and the plate boundary. The force acting on the plate is defined as the pressure difference across the plate, and the pressure, for an inviscid fluid, neglecting gravity and the velocity terms, can be obtained from Bernoulli's equation. The expression for the force is used to find a solution that satisfies both plate and fluid equations to give

$$\rho=\frac{E\upsilon_n^5 d^3}{24\left\{1-\sigma^2\right\}a^5(2\pi f)^2}-\frac{\rho_s d\upsilon_n}{2a}, \tag{1}$$

where ρ is the fluid density and f is the resonance frequency of the plate immersed in the fluid. In a vacuum ($\rho=0$) and Eq. (1) reduces to

$$f(p=0) = (2\pi)^{-1} \left[\frac{E v_n^4 d^2}{12\left\{1-\sigma^2\right\} a^4 \rho_s} \right]^{1/2}, \qquad (2)$$

for the resonance frequency $f(p=0)$. In Eqs. (1) and (2) a is the plate length and d is the plate thickness. Both Eqs. (1) and (2) require values of Young's modulus (E), Possion's ratio (σ), and the density (ρ_s) for the 20 μm silicon plate with an additional thickness of about 2.3 μm consisting of silicon nitride, silicon oxide, and aluminum. Clearly, Eq. (1) requires a precise knowledge of the plate thickness d and plate length a.

The temperature dependence of both Young's modulus and Poisson's ratio were estimated for silicon with a crystallographic plane (1,0,0) (used to fabricate the transducer in this work), as described Ref. [34], from the temperature dependence of the adiabatic stiffness elastic constants obtained from McSkimin [36] and Nikanorov et al. [37]. For the analyses presented here, we have taken the density of silicon to be ρ (Si, 293.15 K, 0.1 MPa) = 2,329.081 kg·m^{-3} based on the values reported by Bettin and Toth [38], Fujii [39], and Waseda and Fujii [40,41]. The variation of density with temperature and pressures ρ (Si, T, p) were obtained using the coefficient of linear thermal expansion and the isothermal compressibility. We have used the linear thermal expansion reported by Swenson [42] and the isothermal compressibility determined from the elastic properties, including the pressure dependence obtained from measurements of the third-order elastic constants reported by McSkimin and Andreatch [43,44]]. The linear thermal expansion coefficient and isothermal compressibility were also used to account for the variation of the plate dimensions a and d with temperature and pressure.

With E, σ, and ρ_s determined from these sources (and described in Ref. [34]) at a temperature of 323 K, Eq. (2) predicts $f(p=0) = 57,886$ Hz which is about 4.7 times the measured value of 12,235 Hz. Equation (1) was used to estimate the resonance frequency [f (calc.)] when the MEMS was exposed to argon at a temperature of 323 K and at 11 pressures between 7 and 68 MPa at which the frequency had been measured f (exp.) (see Table II); the density of argon required in the calculation was determined from the correlation of Tegeler et al. [52]. The ratio f (calc.) to the measured value f (exp.), shown in Fig. 3, is about 4.8. These rather large differences between the estimated and measured frequencies must arise from a combination of practical departures from the assumptions used to derive Eq. (1) and the assumption that the physical properties of the plate are those of silica. Almost all of the effects will be associated with extra dissipation and extra mass in the moving components (such as the silica mounting of the plate) and so it is to be expected that the
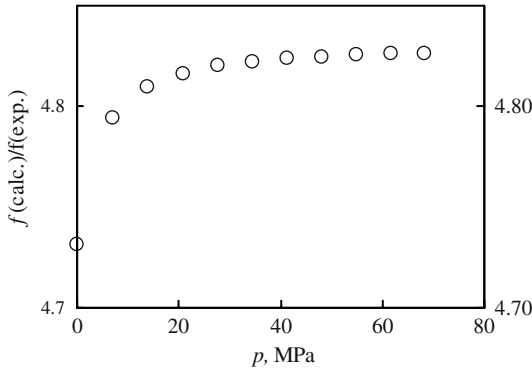
Fig. 3. The ratio f(calc.)/f(exp.) as a function of pressure p. f(calc.) was obtained from Eq. (5) with the mechanical properties of silicon for the edge-supported plate immersed in argon at a temperature of 323.15 K and at pressures between 7 and 68 MPa. f(exp.) is the experimentally determined frequency: ○, f(calc.)/f(exp.).

practical resonance frequency will be below that expected for the ideal sensor. Clearly, without calibration, which will be described in Section 4, the instrument will have a systematic error. There are other aspects of the MEMS design, fabrication, packaging, and operation that can also contribute to the differences between the theoretical and observed resonance frequency. These effects have been discussed in Ref. [34].

The fluid viscosity η was determined from [34]

$$\eta = \frac{C_3}{\rho f^3} \left\{ \frac{2g}{f} - \frac{2g(p=0)}{f(p=0)} \right\}^2 , \qquad (3)$$

where f is the resonance frequency of the plate immersed in the fluid, $f(p=0)$ is the resonance frequency in vacuum, g is half the resonance line-width in the fluid, $g(p=0)$ in a vacuum, ρ is the fluid density obtained from Eq. (1), and C_3 is a constant determined by calibration also described in Section 4.

Ronaldson [45], Manrique de Lara and Atkinson [46], and Manrique de Lara [47] have derived working equations, which are solved numerically, describing the motion of a plate in a fluid using the equation of continuity and the Navier–Stokes equation. The model presented in Ref. [45] will be applied to this MEMS densimeter and viscometer in a future article.

3. APPARATUS AND MEASUREMENTS

The design of the MEMS, shown in Fig. 1, was based on a device reported by Donzier et al. [30]. It was fabricated by École Supérieure d'Ingénieurs en Électrotechnique et Électronique (ESIEE) with methods that are similar to those described by Bourouina et al. [48]. The complete fabrication process has been described elsewhere [34] and only the essential features are provided here. The MEMS was processed on a 101.6 mm diameter silicon-on-insulator wafer (SOI) with a crystallographic plane (1,0,0) that consists of a 20 μm monocrystalline silicon layer fusion-bonded to a silicon oxide layer (about 0.5 μm thick) that isolates the upper layer from the ≈ 350 μm monocrystalline silicon wafer below. About 600 transducers, shown in Fig. 1, were processed on one 101.6 mm diameter wafer. The processes include the use of photolithography (as used in integrated circuit fabrication) and deep reactive ion etching for the micro-machining [49]. Photolithography uses ultraviolet (UV) sensitive material (photoresist) and masks that define shapes and, when this combination is exposed to UV, the resulting patterned surface is chemically etched to remove the unwanted materials deposited onto the wafer to form particular elements, for example, resistors. To actuate and sense the plate motion as well as interconnect with the external electronics, five boron-doped polycrystalline silicon resistors and aluminium wire, shown in Figs. 1 and 2, were deposited atop the 20 μm monocrystalline silicon. Four of these resistors formed a strain gauge configured as a Wheatstone bridge, shown in Figs. 1 and 2, located close to where the 20 μm thick plate will meet the underlying wafer. The fifth resistor could (not used in this work) be used as a temperature detector. The deposited aluminum underwent photolithography to form a wire and provided an excitation coil as well as electrical connections between the wire-bond pads and the bridge and thermometer resistors as well as the coil used to excite motion. The edge-supported plate, that is forced to vibrate, was formed by micromachining to be about 1.45 mm long and 1.8 mm wide. Over the surface area of the plate, the thickness varies from 21.6 to 23 μm with an estimated average thickness over the plate of ≈ 22.25 μm. The MEMS was mounted on a printed circuit board and all but the active element was sealed within a tube using adhesive as described in Ref. [34]. The adhesive limited the upper operating temperature to below 448 K and the upper operating pressure to less than 130 MPa. The upper operating temperature of the MEMS, without packaging, is limited to about 490 K by the boron-doped polycrystalline silicon resistors. The MEMS used for the measurements reported here was not the same device used in Ref. [34] although it was taken from the same wafer.

The MEMS, mounted in its packaging, was placed in a pressure vessel described in Ref. [34] together with a pressure gauge. An electromagnet was formed by winding about 700 turns of polyimide-coated copper wire with a diameter 0.3 mm onto a bobbin that was about 40 mm in length and manufactured from aluminum. It was mounted so that the MEMS plate was in the center of the bobbin. When a dc voltage was passed through the coil, it formed an electromagnet and provided a magnetic field B, shown in Fig. 3, perpendicular to the tip of the vibrating plate. When 25 V dc (at a current of about 1 A) was applied to the coil at $T = 298$ K, a flux of about 0.1 T, determined with a magnetic flux meter, was generated within the center of the bobbin about the location of the plate. The aluminum coil atop the plate was driven with a frequency synthesizer (Agilent Model 33120A), which was phase-locked to a stabilized 10 MHz time-base, with a relative resolution and accuracy of $\approx 10^{-11}$. As $p \to 0$ the frequency synthesizer was set to provide a signal amplitude of 0.15 V ac peak-to-peak (the minimum required to lock with the detector), while at $p > 0$ the voltage was increased to 1 V ac peak-to-peak at the highest densities studied; for a given temperature, this approach maintained about the same signal-to-noise ratio over the whole density range and provided a resonance frequency that was, as we will argue in the digression below, independent of the drive voltage.

When an ac current ($i = 1$ mA in Fig. 3) was in the magnetic field, the plate moved at the frequency of the current as illustrated in Fig. 3. The Wheatstone bridge located near the plate support is supplied with 0.5 V dc and, when the plate is forced to vibrate, the bending motion results in a variation in the resistance of two of the bridge resistors so that an out-of-balance voltage is generated proportional to the displacement velocity. The ac complex voltage generated by the motion of the plate was detected with a lock-in amplifier (Stamford Research Systems Model 850), set at a time constant of 0.3 s, relative to the complex voltage sent to the coil. When the MEMS was immersed in a fluid, $f(T, p)$ and $Q(T, p)\{= f/(2g)\}$ were determined only after three consecutive measurements of T, p, and f, met the following criteria: $\Delta T/T < 10^{-5}$, $\Delta p/p < 10^{-4}$, and $\Delta f/f < 10^{-5}$.

The resonance frequency f and line half-width g of the well-resolved singlet mode (1,0) $\{f(2, 0) \approx 27.5$ kHz at $p = 0\}$ were obtained from measurements of the in-phase $u(f)$ and quadrature $v(f)$ voltages at 11 discrete frequencies from $f - g$ in steps of $g/5$ to about $f + g$ and then back to $f - g$ close to resonance. The parameter g is half the resonance line width defined at frequencies either side of f at which the amplitude is equal to the maximum amplitude divided by $2^{1/2}$. The resonance scan was reversed from $f + g$ to $f - g$ to ensure that temperature drifts, which could lead to a serious error in the measurement of g, had not occurred

during the course of the measurements. After each frequency step, the
system waited a time, which is a multiple of the slowest relaxation time
of the measurement, prior to measuring the complex voltage. In our case,
this time was determined by the post-detection lock-in time constant. The
measured $u(f)$ and quadrature $v(f)$ were fit to a functional form [Eq. (29)
of Ref. [34]] with an algorithm developed by Mehl [50]. The uncertainty
in the determination of the resonance frequency depends on the Q of the
resonance. For values of Q that varied between 64 and 84, our measure-
ments were characterized by a standard deviation in resonance frequency
$\sigma(f) < 0.06$ Hz and a relative difference of $< 14 \times 10^{-6}$.

Before continuing with the description of the apparatus, we digress to
discuss both the amplitude of motion of the plate and the possible volt-
age dependence of the resonance frequency. All of the measurements per-
formed to evaluate these effects were with a magnetic flux of about 0.1 T.

In another article [51], measurements of the plate displacement as a
function of distance z (Fig. 1) along the plate (perpendicular to the sup-
port hinge) were performed when the MEMS device was exposed to both
ambient air and a liquid of viscosity 48 mPa·s. For these measurements
five ac voltages were applied to the coil of 10, 20, 100, 500, and 1,000 mV.
The displacement in the y-direction as a function of z was determined
with a Poly-Tec Vibrometer Model OFV-5000, which contains a laser and
utilizes the Doppler effect to measure the displacement, combined with
a fiber optic-based detector Model OFV-551. As expected, the measured
y-displacement (Fig. 1) at each z increased with increasing voltage and
the displacement of the tip $(z = a)$ increased linearly with the ac voltage
applied to the coil. The y-displacement as a function of z corresponded
with a quarter period of a sinusoidal function in the limit of small ampli-
tude. When the plate was exposed to ambient air, the tip $(z = a$, see Fig. 1)
y-displacement, at a frequency of about 12.9 kHz, increased from 0.05 μm,
when the ac voltage applied to the coil was 10 mV, to 6 μm, when the
ac voltage applied to the coil was 1 V. The y-displacement was also mea-
sured parallel (and close to the hinge $z \approx 0$ in Fig. 1) in the x direction
with an ac voltage of 0.5 V applied to the coil. The y-displacement was
greatest at $x/2$, the center of the plate, but never differed by more than
1% from center to edge. The displacement measurements were repeated
with the MEMS device immersed in silicon oil with a nominal viscosity
of 48.4 mPa·s. In this fluid, the tip $(z = a$ shown in Fig. 1) displacement
was about 77 nm when the voltage applied to the coil was 1 V ac. This is
a factor of 78 less than observed when the MEMS device was exposed to
air at ambient conditions.

These measurements show that the amplitude of the plate motion is
about 3 μm when 0.5 V ac is applied to the coil; this voltage was used in

this work at pressures above 7 MPa. This amplitude is less than the plate thickness (22 μm) by a factor of about 10 and a factor of 500 less than the plate length. The Reynolds number is defined by

$$Re = vL\rho/\eta, \tag{4}$$

where v is the fluid speed and L is an appropriate length. If we assume the amplitude of the plate oscillation is equal to the oscillations of the fluid close to the plate, then $L = 3 \times 10^{-6}$. Based on the same assumption, the estimated fluid velocity is $v = 0.07 \, \text{m} \cdot \text{s}^{-1}$. For argon at a temperature of 323 K and pressure of 7 MPa, the viscosity is 27 μPa·s and the density 107 kg·m^{-3} and under these conditions Eq. (4) gives $Re = 0.8$ so that the flow of fluid about the plate is considered slow and laminar.

In this work, we have also measured the resonance frequency of the device in argon (at $T = 323$ K and $p = 0.7$ MPa where $\rho = 10.5 \, \text{kg} \cdot \text{m}^{-3}$ and $\eta = 24.3 \, \mu\text{Pa} \cdot \text{s}$) as a function of the ac voltage applied to the coil of between 0.25 and 0.5 V; the dc voltage applied to the Wheatstone bridge was kept constant during these measurements at 0.5 V dc. Under these conditions (which is the worst case experienced in this work), the relative difference in the measured resonance frequency obtained with these two sinusoidal voltages was less than 10^{-5}. At the same temperature and pressure at which these measurements were performed, a relative difference in frequency of $\pm 3 \times 10^{-4}$ results in a relative variation in the density obtained from the device of $\pm 0.1\%$. This variation of frequency with applied coil voltage was not detectable when the MEMS was immersed in a liquid as it was for the measurements reported in Ref. [34].

Based on a combination of both these observations and the estimated Reynolds number, we conclude the voltage dependence of the resonance frequency of the MEMS device surrounded by argon with less than 1 V ac applied to the coil is not a source of a significant systematic error in our measurements.

We also measured the resonance frequency as a function of both the voltages applied to the coil and the Wheatstone bridge with the MEMS device exposed to a low pressure of about $5 \cdot 10^{-3}$ Pa that we approximate as a vacuum; the pressure was determined with an ionization gauge separated from the MEMS by about 1 m length of 0.8 mm inner diameter tube. In the first series of experiments, the voltage applied to the coil was maintained at 1 V ac while the voltage applied to the bridge was varied from 0.5 to 6 V dc in steps of 0.5 V dc. As expected, the measured resonance frequency was invariant over this range of dc voltages. For a second series of experiment, we maintained the voltage applied to the bridge at 0.5 V dc while varying the voltage applied to the coil from 0.3 to 5 V ac; at voltages

between 0.3 and 1 V ac, a step of 0.1 V was used while for the range 1–5 V ac a step size of 0.5 V was used. For these variables, we observed a frequency proportional to V^{-1} as anticipated based on the performance of other vibrating object densimeters/viscometers. When our MEMS device was operated in a vacuum, the minimum voltage applied to the coil was always 0.15 V ac, and based on these measurements, we concluded that the constant voltage introduced a negligible additional uncertainty in the measured frequency. We now return to describe the measurements of temperature and pressure.

Both the MEMS and the pressure gauge were thermostated in a stirred fluid bath, and the temperature of the bath fluid determined on ITS-90 with a long-stem platinum resistance thermometer with a resolution of ± 1 mK and an accuracy, at each temperature, specified by ITS-90. During the time required to measure the resonance frequency, the temperature of the bath fluid varied, in the worst case, by about $\delta T = 3$ mK. Here we assume that the δT for the fluid to which the MEMS is exposed is equal to that of the bath fluid. This upper bound for δT results in a negligible uncertainty of $\delta \rho < 6 \times 10^{-3}$ kg·m^{-3} (contribution less than 0.01%) in density because for the fluids investigated over the range of conditions experienced $|(\partial \rho / \partial T)_p| < 2$ kg·m^{-3}·K^{-1}. This $\delta T \approx 3 \times 10^{-3}$ K also gives rise to an insignificant ($< 0.001\%$) variation in viscosity on the reasonable assumption that $|(\partial \eta / \partial T)_p| < 0.1 \, \mu$Pa·s·K^{-1}.

Pressures were measured with a resonant quartz transducer which, when calibrated against an oil-lubricated dead-weight gauge, was found to have an uncertainty of $\delta p / \text{MPa} = \pm \{1 \times 10^{-4}(p/\text{MPa}) + 0.022\}$. In the temperature and pressure range investigated here, $\delta p \approx 0.029$ MPa, and when combined in the worst case with $(\partial \rho \, (\text{Ar}, 323 \, \text{K}, 7 \, \text{MPa})/\partial p)_T \approx 15.5$ kg·m^{-3}·MPa^{-1}, corresponds to a potential uncertainty in density of 0.45 kg·m^{-3} (or about 0.4%). The value of $\{\partial \rho \, (\text{Ar}, T, p)/\partial p\}_T$ decreases with increasing temperature to 11 kg·m^{-3}·MPa^{-1} at $T = 423$ K and $p = 7$ MPa and also decreases with pressure to 6 kg·m^{-3}·MPa^{-1} at $T = 323$ K and $p = 68$ MPa. Thus, the pressure measurement introduces an estimated uncertainty in our knowledge of the fluid density of about 0.4% at $T = 323$ K and $p = 7$ MPa, 0.2% at $p \approx 14$ MPa, and about 0.1% at $p \approx 20$ MPa; at $T = 423$ K and $p = 68$ MPa the same δp introduces an uncertainty of $< 0.03\%$ in density. For viscosity $(\partial \eta / \partial p)_T < 0.5 \, \mu$Pa·s·MPa^{-1}, and $\delta p \approx 0.029$ MPa of the pressure gauge corresponds to a negligible uncertainty in viscosity of $< 0.03\%$. In a future article we will show that the MEMS can, as anticipated from Eq. (1) that shows the density is inversely proportional to f^2, operate at pressures below 10 MPa [34]. Pressures were generated with an ISCO Model 100 DX positive displacement pump with

an upper operating pressure of about 68 MPa, which limited the upper operating pressure of the MEMS.

The density, viscosity, and their derivatives with respect to pressure and temperature for argon were determined with the Helmholtz function reported by Tegeler et al. [52] and the transport property correlation of Lemmon and Jacobsen [53] as coded within the National Institute of Standards and Technology, Standard Reference Database 23, Version 7.1 commonly known by the acronym REFPROP [54].

Prior to measurements with each fluid, the apparatus was evacuated with a turbo-molecular pump to a pressure (as indicated by an ionization gauge located near the pump) of less than $< 10^{-2}$ Pa for at least 24 h. The pressure within the apparatus where the MEMS is located could have been considerably different resulting from the high pumping impedance of the high-pressure tube that is about 1 m long and has an internal diameter of 0.8 mm.

The argon was supplied by Praxair Inc., Danbury, CT, with a mole fraction purity stated by the supplier of greater than 0.999999. No further analysis of the chemical composition was performed.

4. CALIBRATION AND UNCERTAINTY

The plate consists of 20 μm mono-crystalline silicon on to which are deposited layers of aluminum, silicon nitride, silicon oxide, and a final protective layer with fabrication processes that require thermal cycling and chemical etching. In Ref. [34] we compared the elastic properties obtained for vapor-deposited materials with those of the bulk stoichiometric substance and found variations as large as a factor of two. Therefore, it is perhaps unreasonable to assume that Young's modulus, Poissons' ratio, and the density of the plate will be equal to those obtained for silicon of $E \approx$ 129 GPa, $\sigma \approx 0.265$, and $\rho \approx 2328$ kg·m^{-3}, respectively. However, in Ref. [51] the Youngs's modulus for a MEMS device, taken from the same batch as the transducer used for the measurements reported here, was measured with the result $E = 125.8$ GPa at a temperature of 323 K. This result is consistent with our assumption and, consequently, we used the value of E, σ, and ρ for silicon. In the absence of direct measurement of σ and ρ and our inadequate knowledge of the dimensions a and d, two additional and unknown parameters C_1 and C_2 are included in Eq. (1) to give

$$\rho = \frac{C_2 E \upsilon_n^5 d^3}{24 \left\{1 - \sigma^2\right\} a^5 \left(2\pi f\right)^2} - \frac{C_1 \rho_s d \upsilon_n}{2a}. \tag{5}$$

The parameters C_1 and C_2 must be determined by calibration with a fluid of known density.

Table I. Resonance Frequency f, Resonance Line Half-Width g and Quality Factor $Q\{= f/(2g)\}$ at Temperature T and Pressure. (Uncertainties in f and g determined from the fit of the in-phase and quadrature voltages measured as a function of frequency are at $k=1$)

T(K)	$f(p \to 0)$, (Hz)	$g(p \to 0)$, (Hz)	Q
$323.163^a \pm 0.003$	$12,234.5223 \pm 0.0026$	2.1733 ± 0.0026	$2,814.734$
348.148 ± 0.003	$12,213.8713 \pm 0.0056$	3.1221 ± 0.0056	$1,956.035$
398.106 ± 0.003	$12,179.6660 \pm 0.0082$	4.0149 ± 0.0082	$1,516.808$
423.111 ± 0.003	$12,151.817 \pm 0.027$	11.151 ± 0.027	544.89
423.110 ± 0.003	$12,152.1494 \pm 0.0056$	13.7906 ± 0.0056	440.595

^{a} Used to determine $C_1 C_2$, and C_3.

To determine C_1 and C_2, the resonance frequency f and the resonance half line-width g were measured at a temperature of 323 K in vacuo (Table I) and when the plate was immersed in argon (Table II) at pressures below 68 MPa. The resonance frequencies, omitting from the regression those determined at pressures below 20 MPa, for which $\delta p \approx 0.029$ MPa contributed an uncertainty in density [52] of up to 0.45 kg·m^{-3} (about 0.4%), were combined with both the elastic properties, described above and in Ref. [34], and the density estimated from the correlation reported by Tegeler et al. [52] (with our measurements of temperature and pressure) to obtain C_1 and C_2 of Eq. (5). This regression was also constrained so that the resonance frequency measured as $p \to 0$ was also reproduced by

$$f(p=0) = (2\pi)^{-1} \left[\frac{C_2 E v_n^4 d^2}{12 \{1-\sigma^2\} a^4 \rho_s C_1} \right]^{1/2}, \qquad (6)$$

with the same C_1 and C_2. Equation (6) was obtained from Eq. (5) and is equivalent to Eq. (2) modified to include the coefficients C_1 and C_2. The parameter C_3 of Eq. (3) was determined by regression with the resonance frequencies and half the resonance line widths. In both regressions the density and viscosity of argon were obtained from Refs. [52] and [53], respectively, using REFPROP [54]. The determined values of $C_{i's}$ with $i = 1$, 2, and 3, are listed in Table III. The density of the stochiometric bulk materials that are deposited atop the silicon are greater than that of silicon and thus one might expect C_1 to be greater than unity; however, the deposited materials are probably neither stochiometric nor of the same crystal structure as the bulk material and thus C_1 determined from the measurements, which is about 4% below unity, is considered reasonable. The elastic properties of the additional layers are less than those of silicon [34], and presumably when combined with the processes

Table II. Density ρ and Viscosity η of Argon Determined from the MEMS Resonance Frequency f with Eq. (5) and The Resonance Line Half-Width g with Eq. (3) as a Function of Pressure p at the Mean Temperatures $<T>$. (Uncertainties in f and g are at $k=1$ while those for density and viscosity are at $k=2$.)

$<T(K)>$	p(MPa)	f(Hz)	G(Hz)	ρ(kg·m^{-3})	η(mPa·s)
323.162^a ± 0.003	7.006 ± 0.023	7,592.457 ± 0.024	45.030 ± 0.024	107.17 ± 0.76	27.44 ± 0.86
	13.877 ± 0.023	5,982.621 ± 0.018	36.467 ± 0.018	213.45 ± 0.93	29.79 ± 0.88
	20.899 ± 0.024	5,116.164 ± 0.015	31.385 ± 0.015	316.3 ± 1.1	32.57 ± 0.94
	27.679 ± 0.025	4,594.231 ± 0.020	28.321 ± 0.020	408.2 ± 1.3	35.2 ± 1.0
	34.459 ± 0.025	4,243.095 ± 0.009	26.486 ± 0.009	489.8 ± 1.5	38.2 ± 1.1
	41.249 ± 0.026	3,993.477 ± 0.012	25.373 ± 0.012	561.2 ± 1.7	41.5 ± 1.2
	48.119 ± 0.027	3,806.221 ± 0.020	24.653 ± 0.020	624.2 ± 1.8	44.8 ± 1.3
	54.885 ± 0.027	3,664.061 ± 0.017	24.187 ± 0.017	678.5 ± 1.9	48.1 ± 1.4
	61.690 ± 0.028	3,551.055 ± 0.011	23.872 ± 0.011	726.2 ± 2.1	51.2 ± 1.5
	68.312 ± 0.029	3,461.187 ± 0.010	23.671 ± 0.010	767.5 ± 2.2	54.2 ± 1.6
348.148 ± 0.003	6.978 ± 0.023	7,802.741 ± 0.031	47.937 ± 0.031	97.69 ± 0.69	29.04 ± 0.91
	17.496 ± 0.024	5,706.091 ± 0.038	36.689 ± 0.038	241.15 ± 0.93	33.08 ± 0.97
	27.653 ± 0.025	4,799.616 ± 0.017	30.617 ± 0.017	368.7 ± 1.2	35.8 ± 1.0
	34.469 ± 0.025	4,428.441 ± 0.036	28.384 ± 0.036	444.9 ± 1.4	38.1 ± 1.1
	41.288 ± 0.026	4,160.309 ± 0.040	26.925 ± 0.040	513.1 ± 1.5	40.7 ± 1.2
	48.154 ± 0.027	3,957.118 ± 0.020	25.963 ± 0.020	574.3 ± 1.7	43.4 ± 1.2
	54.879 ± 0.027	3,801.964 ± 0.014	25.330 ± 0.014	627.8 ± 1.8	46.3 ± 1.3
	61.690 ± 0.028	3,676.291 ± 0.016	24.858 ± 0.016	676.3 ± 1.9	49.0 ± 1.4
	68.529 ± 0.029	3,573.405 ± 0.013	24.362 ± 0.013	719.8 ± 2.0	51.0 ± 1.5
398.106 ± 0.003	7.360 ± 0.023	8,014.974 ± 0.021	49.520 ± 0.021	88.47 ± 0.60	29.20 ± 0.91
	13.876 ± 0.023	6,560.923 ± 0.013	42.416 ± 0.013	165.12 ± 0.71	31.38 ± 0.92
	27.719 ± 0.025	5,107.467 ± 0.010	33.654 ± 0.010	316.2 ± 1.0	36.2 ± 1.0
	34.448 ± 0.025	4,718.134 ± 0.020	31.349 ± 0.020	382.2 ± 1.2	38.6 ± 1.1
	41.294 ± 0.026	4,425.7777 ± 0.029	29.893 ± 0.029	443.6 ± 1.3	41.7 ± 1.2
	48.140 ± 0.027	4,201.613 ± 0.047	28.632 ± 0.047	499.6 ± 1.5	44.1 ± 1.3

Table II. Continued.

$<T(K)>$	p(MPa)	f(Hz)	G(Hz)	ρ(kg·m^{-3})	η(mPa·s)
	54.949±0.027	4,025.362±0.015	27.735±0.015	550.4±1.6	46.6±1.3
	61.785±0.028	3,882.163±0.008	27.068±0.008	596.9±1.7	49.1±1.4
423.112±0.003	7.008±0.023	8,252.082±0.042	56.855±0.042	79.27±0.55	31.13±0.98
	14.381±0.023	6,613.164±0.027	48.214±0.027	160.69±0.68	33.98±1.00
	21.065±0.024	5,778.916±0.030	42.479±0.030	231.06±0.81	36.1±1.0
	27.779±0.025	5,223.881±0.022	38.496±0.022	297.59±0.96	38.1±1.1
	34.529±0.025	4,826.990±0.016	35.705±0.016	359.8±1.1	40.3±1.2
423.110±0.003	7.272±0.023	8,174.183±0.047	57.338±0.047	82.13±0.56	29.96±0.94
	14.124±0.023	6,657.650±0.043	48.867±0.043	157.84±0.67	32.14±0.95
	21.056±0.024	5,782.557±0.035	42.838±0.035	231.04±0.81	34.2±1.0
	27.786±0.025	5,225.748±0.018	38.690±0.018	297.92±0.96	35.9±1.0
	34.605±0.025	4,825.152±0.020	35.779±0.020	361.0±1.1	37.6±1.1
	41.249±0.026	4,533.826±0.025	33.779±0.025	417.7±1.2	39.8±1.1
	48.197±0.027	4,297.790±0.040	32.253±0.040	472.3±1.4	42.1±1.2
	48.189±0.027	4,298.062±0.029	32.175±0.029	472.3±1.4	41.8±1.2
	55.018±0.028	4,114.132±0.016	31.171±0.016	521.5±1.5	44.4±1.3
	61.834±0.028	3,964.935±0.035	30.332±0.035	566.5±1.6	46.7±1.4
	68.620±0.029	3,840.912±0.025	29.749±0.025	608.0±1.7	49.3±1.4

[a] Used to determine C_1, C_2, and C_3.

Table III. Values of C_i, with $i = 1$, 2, and 3, of Eqs. (5) And (3) Obtained from Measurements with Argon at a Temperature of 323.15 K, Listed in Table II, at Pressures Between 20 and 68 MPa along with f (323 K, $p \rightarrow 0$) of Table I

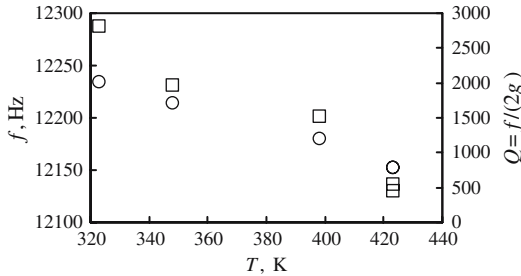| T(K)	C_1	C_2	C_3 (kg^2·m^{-4}·s^{-5})
323.15	0.95751141	4.277367×10^{-2}	$9.719654446 \times 10^{12}$

Fig. 4. Resonance frequency f and quality factor Q of the (1,0) fundamental mode of the edge-supported plate as a function of temperature at a pressure of about 5×10^{-3} Pa: $\bigcirc$, f; and $\square$, Q.

used to fabricate the MEMS, have drastically reduced the actual E and σ as suggested by a coefficient C_2 of about 0.04. In our previous paper [34], we reported measurements with methylbenzene and octane obtained with another MEMS from the same wafer as the device used for the measurements reported here. In Ref. [34] the MEMS was calibrated by immersion in methylbenzene; and $C_1 \approx 0.89$, $C_2 \approx 3.8 \times 10^{-2}$, and $C_3 \approx 9.3 \times 10^{12}$ kg^2·m^{-4}·s^{-5} were determined based on the density and viscosity of methylbenzene obtained from the correlation of Assael et al. [55] The C_i's of Ref. [34] are about 6% lower for C_1 and C_2 and 4% lower for C_3 than those listed in Table III. In Eqs. (3), (5), and (6) we have assumed that C_i's, with $i = 1$, 2, and 3, are independent of T, p, η, and ρ.

The first term of Eq. (5) contributes between 174.3 and 834.6 kg·m^{-3} to the measured density that arises mostly from the variations in resonance frequency while the second term varies by 0.04 kg·m^{-3}, a variation that arises solely from the pressure dependence of both the density and elastic properties of silicon.

The measured resonance frequencies, f, and quality factors, Q, obtained in vacuo as a function of temperature in the range 323–423 K are shown in Fig. 4. As expected, f and Q decrease with increasing

temperature. The resonance frequencies as $p \to 0$ are shown in Fig. 5 as fractional deviations from the values obtained from Eq. (2) with C_1 and C_2 of Table III and never exceed 0.26%. However, the values of $Q(p \to 0)$ listed in Table I are significantly lower (at least a factor of 10) than anticipated from the measurements reported for cantilevers by Blom et al. [56] and Yasumura et al. [57] and from preliminary calculations for our plate. At a pressure of about 1 Pa, the Q's reported in Ref. [58] are about the same order of magnitude as those listed in Table I. As noted earlier, the pressure within our apparatus could have been considerably higher than the pressure of $< 10^{-2}$ Pa measured with an ionization gauge as a result of the high pumping impedance of the high-pressure tube. For that reason, we do not with a length of 1 m and an internal diameter of 0.8 mm consider the experimental values of Q unreasonable.

The densities determined from Eq. (5) at a temperature of 323 K using C_1 and C_2 from Table II are shown in Fig. 6 as relative deviations from the values obtained from the correlation of Tegeler et al. [52]. The uncertainty in density predicted from Ref. [52] has been cited as $< 0.02\%$ for pressures up to 12 MPa and temperatures up to 340 K with the exception of the critical region and the uncertainty is $< 0.03\%$ for pressures up to 30 MPa and temperatures between 235 and 520 K. Elsewhere, the uncertainty in density is within 0.2%. The uncertainty of the density obtained from Ref. [53] is shown in Fig. 7 with dashed lines. At $p > 14$ MPa (the pressures used to obtain C_1 and C_2) the measured densities deviate by less than $\pm 0.04\%$ from the correlation [52], which is within the uncertainty of Ref. [52]. At $p < 14$ MPa the deviations of our results from Ref. [52] increase with decreasing pressure to 0.6% at $p \approx 7$ MPa. A plausible explanation for this observation is obtained from the uncertainty of our pressure gauge of $\delta p \approx 0.029$ MPa which, at pressures below 20 MPa, contributed an uncertainty in the density (estimated using Ref. [52]) of up to 0.45 kg·m^{-3} (about 0.4%). No experiments were performed to specifically verify this possibility. However, the estimated expanded ($k = 2$) uncertainty (discussed in Section 6), including the uncertainty in density arising from the pressure gauge, increase, as shown in Fig. 6, with decreasing pressure to about 0.7% at $p \approx 7$ MPa. Thus, we take the average of the absolute differences of our measurements at $p > 14$ MPa from the correlation [52] of $\pm 0.02\%$ as a measure of the estimated uncertainty in the density determined with this instrument.

The viscosities were determined at $T = 323$ K from Eq. (3) with the measured Q combined with C_3, listed in Table III, and the densities estimated from Eq. (5) are shown in Fig. 7 as relative deviations from the correlation of Lemmon and Jacobsen [53]. The uncertainty in viscosity obtained from Ref. [53] varies between 0.5% at pressures below 1 MPa to
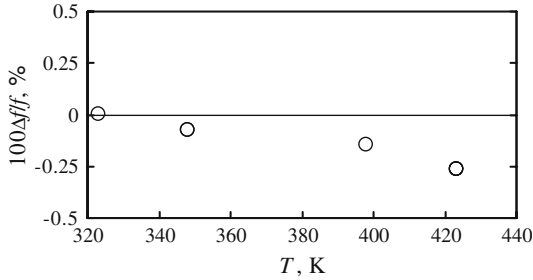
Fig. 5. Relative fractional differences $\Delta f/f = \{f(\text{expt.}) - f(\text{calc.})\}/f(\text{calc.})$ of the experimentally determined resonance frequency $f(\text{expt.})$ from the calculated resonance frequency $f(\text{calc.})$ determined from Eq. (6): $\bigcirc$, f.

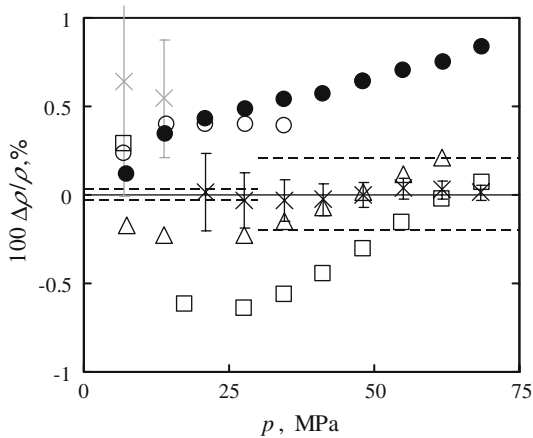**Fig. 6.** Fractional deviations $\Delta\rho/\rho = \{\rho(\text{expt.}) - \rho(\text{calc.})\}/\rho(\text{calc.})$ of the experimental densities ρ (expt.) of argon listed in Table II from values ρ (calc.) obtained with the correlation of Tegeler et al. Tegeler et al. [52], with our experimental temperatures and pressures, as a function of pressure p. $\times$, $T = 323.16\,\text{K}$ used to obtain C_1 and C_2 of Table III; $\times$, $T = 323.16\,\text{K}$ not used to determine C_1 and C_2 because $\delta p \approx 0.029\,\text{MPa}$ gives rise to a corresponding error $\delta\rho$ of up to $0.45\,\text{kg}\cdot\text{m}^{-3}$, according to [52]: $\square$; $T = 348.15\,\text{K}$; $\triangle$, $T = 398.11\,\text{K}$; $\bullet$, $T = 423.11\,\text{K}$; $\bigcirc$, $T = 423.11\,\text{K}$; and $----$, uncertainty of the correlation [53].
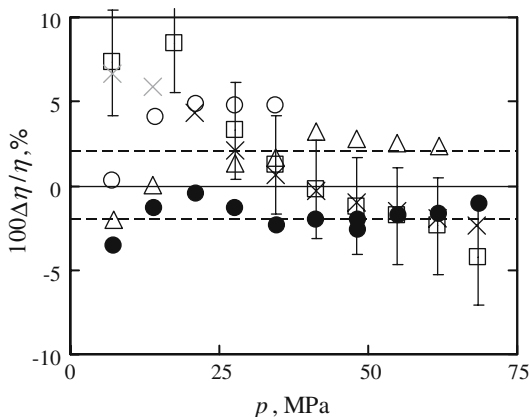
Fig. 7. Fractional deviations $\Delta\eta/\eta = \{\eta(\text{expt.}) - \eta(\text{calc.})\}/\eta(\text{calc.})$ of the experimental viscosities $\eta(\text{expt.})$ of argon listed in Table II from values $\eta(\text{calc.})$ obtained with the correlation of Lemmon and Jacobsen [53], with our experimental temperatures and pressures, as a function of pressure p. $\times$, $T = 323.16\,\text{K}$ used to obtain C_3 Table III; $\times$, $T = 323.16\,\text{K}$ not used to determine C_3 because $\delta p \approx 0.023\,\text{MPa}$ gave rise to a corresponding error $\delta\rho$ of about $0.45\,\text{kg·m}^{-3}$, according to [52], and the determination of η with Eq. (3) used ρ from Eq. (5): $\square$; $T = 348.15\,\text{K}$; $\triangle$, $T = 398.11\,\text{K}$; $\bullet$, $T = 423.11\,\text{K}$; $\bigcirc$, $T = 423.11\,\text{K}$; and ----, uncertainty of the correlation [53].

1% at temperatures between 270 and 300 K and pressures below 100 MPa and increases to about 2% at temperatures and pressures corresponding to the range of the measurements reported here. The viscosity obtained from Ref. [53] at pressures below 1 MPa differs by less than 2% from values estimated from the correlations reported by Maitland et al. [59]. The uncertainty of the viscosity obtained from Ref. [53] is shown in Fig. 7 with dashed lines. At $p > 14\,\text{MPa}$, the measurements used to obtain C_3, the deviations of our results from Ref. [53] vary from –2.3% at $p \approx 68\,\text{MPa}$ to 4.3% at $p \approx 21\,\text{MPa}$. At $p < 14\,\text{MPa}$ the deviations of our results from Ref. [53] increase with decreasing pressure to be 6.7% at $p \approx 7\,\text{MPa}$, which is attributed to the uncertainty in the density obtained from Eq. (5) and not to the uncertainty in our pressure gauge of $\delta p \approx 0.029\,\text{MPa}$ that contributed an uncertainty in the viscosity of $< 0.03\%$. In Fig. 7, our results, shown with $\times$, lie within $\pm 5\%$ of Ref. [53]. Again, we take the average of the absolute differences between our measurements at $p > 14\,\text{MPa}$

from Ref. [53] of $\pm 1.4\%$ as a measure of the estimated uncertainty in the viscosity determined with this device.

For the measurements reported here the viscosity varies from 26 to 56 mPa·s and the density from 79 to 767 kg·m^{-3} and the assumption that the density and viscosity can be represented by independent equations is probably not a significant source of error particularly when C_i'$_s$ with $i =$ 1, 2, and 3 are determined using a fluid with viscosities and densities that include these ranges.

5. RESULTS

The resonance frequency, f, and half the resonance line width, g, of the first eigenmode of the edge-supported plate that were measured while it was immersed in argon at temperatures between 348 and 423 K at pressures below 68 MPa are listed in Table II. The density and viscosity, also listed in Table II, were obtained from Eqs. (5) and (3), respectively, with the f and g of Table II combined with the C_1, C_2, and C_3 of Table III, determined solely at a temperature of 323 K. In the analysis, the temperature and pressure dependence of the plate dimensions and the density and elastic constants of silicon were included as described in Ref. [34]. The density obtained from Eq. (5) from the MEMS f was used in Eq. (3) to determine the viscosity. Small corrections have been applied to the viscosity and density reported in Table II to reduce all values to the stated temperature for each isotherm.

The combined expanded uncertainties, listed in Table II, are for a coverage factor $k = 2$, that assuming a normal distribution represents a confidence interval of about 0.95, and were obtained by combining in-quadrature standard uncertainties arising from the transducer calibration with $(\partial \eta / \partial T)_p$ and $(\partial \eta / \partial p)_T$ for viscosity and $(\partial \rho / \partial T)p$ with $(\partial \rho / \partial p)_T$ for density.

For the viscosity we have also included the uncertainty in density obtained from Eq. (5). Not surprisingly, for both density and viscosity the major source of uncertainty arises from the uncertainty of the calibration that is, based on the average absolute uncertainties obtained from the calibration; 0.04% for density and 1.4% for viscosity. The next most significant and quantifiable contribution to the uncertainties arises from $(\partial \eta / \partial p)_T$ for viscosity and $(\partial \rho / \partial p)_T$ for density. These derivatives were estimated from a combination of our results and the uncertainty in the pressure measurement, δp, listed in Table II. The contribution to the uncertainty in viscosity, $\delta \eta$, from δp was less than 0.02 mPa·s (about 0.07%) that decreased with increasing temperature, while the density error, $\delta \rho$, from δp was less than 0.44 kg·m^{-3} (about 0.4%) at $p \approx 7$ MPa and less

than 0.02% at $p \approx 68$ MPa. The contribution to the uncertainty from either $(\partial\eta/\partial T)_p$ or $(\partial\rho/\partial T)_p$ was estimated from a combination of our results and the uncertainties in the temperature δT listed in Table II. The contribution to $\delta\eta$ from δT was less than $\pm 2 \times 10^{-4}$ mPa·s (about 8×10^{-4}%) and from $\delta\rho$ less than 6×10^{-3} kg·m^{-3} (about 10^{-3}%). Clearly, for our measurements the uncertainty with which the pressure is measured is more significant than the uncertainty in our determination of temperature. In the absence of a chemical analysis for these fluids, and based on the purity of the argon as specified by the supplier, the contribution to the uncertainty arising from the uncertainty in composition was assumed to be negligible.

The working equations explicitly assume that the density and viscosity are represented by independent equations. In the absence of sufficient additional measurements with fluids of different densities and viscosities to determine the uncertainty from this source, we have also assumed the contribution to the estimated uncertainty from our zeroth-order model is negligible.

At all densities in the temperature range from 323–423 K, the relative deviations of our results from Ref. [52] fall within ± 0.8% (Fig. 6), and at $\rho > 200$ kg·m^{-3} the deviations are less than 1% although showing systematic deviations as a function of pressure. At $\rho < 200$ kg·m^{-3} the deviations, also shown in Fig. 6, increase with decreasing density consistent with the known uncertainty in the measured pressure used to predict ρ. This agreement is quite remarkable given the simplicity of Eq. (5) and the density range of 100–800 kg·m^{-3} over which measurements were performed. The deviations, shown in Fig. 6, have no significant temperature dependence. The measurements of density at $T = 423$ K were repeated and found to be self-consistent to within < 0.1%.

The values of viscosity are shown in Fig. 7 as relative deviations from the correlation of Lemmon and Jacobsen [53]. In this case the η obtained, with one temperature independent coefficient, at temperatures of 348, 398, and 423 K all lie within ± 10%. This rather good agreement, in light of the observations made for density, is probably fortuitous. The two series of viscosity measurements at $T = 423$ K provided results that differed by about 5%, which is less than twice the estimated expanded uncertainty of the measurements.

The relative fractional deviations shown in Figs. 6 and 7 might arise from one or more of the following plausible sources: the simplicity of Eqs. (5) and (3), especially the assumption that the density can be represented by an expression independent of viscosity [the inviscid assumption used to obtain Eq. (5)]; and the arbitrary use of only three calibration parameters, two for density and one for viscosity. Here we have assumed the correlations used to obtain the deviations are exact.

6. CONCLUSIONS

Our intent was to fabricate a densimeter/viscometer that can operate at petroleum reservoir conditions (at temperatures < 473 K and pressures < 200 MPa) and provide results with an uncertainty in both properties sufficient (approximately 1% in density and 10% in viscosity) to guide value and exploitation calculations with sufficient rigor. Under these conditions robustness was given a higher priority in the design than assigned to accuracy. Nevertheless, when the MEMS was immersed in argon at temperatures between 348 and 423 K and at pressures below 68 MPa, the density and viscosity were obtained from the measured complex frequency with an estimated relative combined expanded ($k = 2$) uncertainty, including the calibration, of about $\pm 0.35\%$ for density and $< \pm 3\%$ for viscosity. Presumably these uncertainty levels will decrease with improvements to the working equations [45–47]. The goals of determining the density to $\pm 1\%$ and the viscosity to $\pm 10\%$ have been achieved within the constraints of the upper operating pressure determined by the positive displacement pump, the lower operating pressure determined by uncertainty of the pressure measurement ($\delta p \approx 0.029$ MPa), and the upper operating temperature determined by the adhesive used in the packaging of the MEMS [34]. The uncertainty, $\delta p \approx 0.029$ MPa for our pressure gauge, corresponds to a maximum uncertainty in density of 0.45 kg·m^{-3} (or about 0.4%) and an uncertainty in viscosity of $< 0.03\%$, which decreases with increasing pressure and temperature.

REFERENCES

1. W. Wagner, R. Kleinrahm, H. W. Lösch, J. T. R. Watson, V. Majer, A. A. H. Pádua, L. A. Woolf, J. C. Hoslte, A. M. de Figueiredo Palavara, K. Fujii, and J. W. Stansfeld, in *Experimental Thermodynamics Vol. VI, Measurement of the Thermodynamic Properties of Single Phases*, A. R. H. Goodwin, K. N. Marsh, and W. A. Wakeham, eds. (Elsevier for International Union of Pure and Applied Chemistry, Amsterdam, 2003), Chap. 5, pp. 127–235.
2. W. Wagner and R. Kleinrahm, *Metrologia* **41**:S24 (2004).
3. N. Kuramoto, K. Fujii, and A. Waseda, *Metrologia* **41**:S84 (2004).

4. V. Majer and A. A. H. Pádua, in *Experimental Thermodynamics Vol. VI, Measurement of the Thermodynamic Properties of Single Phases*, A. R. H. Goodwin, K. N. Marsh, and W. A. Wakeham, eds. (Elsevier for International Union of Pure and Applied Chemistry, Amsterdam, 2003), Chap. 5, pp. 158–168.

5. J. W. Stansfeld, in *Experimental Thermodynamics Vol. VI, Measurement of the Thermodynamic Properties of Single Phases*, A. R. H. Goodwin, K. N. Marsh, and W. A. Wakeham, eds. (Elsevier for International Union of Pure and Applied Chemistry, Amsterdam, 2003), Chap. 5, pp. 208–225.

6. J. F. Johnson, J. R. Martin, and R. S. Porter, in *Physical Methods of Chemistry*, Pt. VI, A. L. Weissberger and B. W. Rossiter, eds. (Interscience, New York, 1977), p. 63.

7. W. Künzel, H. F. van Wijk, and K. N. Marsh, in *Recommended Reference Materials for the Realization of Physicochemical Properties*, K. N. Marsh, ed. (Blackwell Scientific for International Union of Pure and Applied Chemistry, Oxford, United Kingdom, 1987), pp. 45–72.

8. J. C. Nieuwoudt and I. R. Shankland, in *Experimental Thermodynamics*, *Vol. III*, *Measurement of the Transport Properties of Fluids*, W. A. Wakeham, A. Nagashima, and J. V. Sengers, eds. (Blackwell Scientific for International Union of Pure and Applied Chemistry, Oxford, United Kingdom, 1991), Chap. 2, pp. 9–48.

9. M. Kawata, K. Kurase, A. Nagashima, and K. Yoshida, in *Experimental Thermodynamics Vol. III, Measurement of the transport properties of fluids*, W. A. Wakeham, A. Nagashima, and J. V. Sengers, eds. (Blackwell Scientific for International Union of Pure and Applied Chemistry, Oxford, United Kingdom, 1991) Chap. 3, pp. 51–75.

10. M. Kawata, K. Kurase, A. Nagashima, K. Yoshida, and J. D. Isdale, in *Experimental Thermodynamics Vol. III, Measurement of the transport properties of fluids*, W. A. Wakeham, A. Nagashima, and J. V. Sengers, eds. (Blackwell Scientific for International Union of Pure and Applied Chemistry, Oxford, United Kingdom, 1991), Chap. 5, pp. 97–110.

11. D. E. Diller and P. S. van der Gulik, in *Experimental Thermodynamics Vol. III, Measurement of the transport properties of fluids*, W. A. Wakeham, A. Nagashima, and J. V. Sengers, eds. (Blackwell Scientific for International Union of Pure and Applied Chemistry, Oxford, U.K., 1991), Chap. 4, pp. 79–94.

12. J. G. Woodward, *J. Acoust. Soc. Am.* **25**:147 (1953).

13. M. K. Andrews and P. D. Harris, *Sens. Actuators A* **49**:103 (1995).

14. S. J. Martin, M. A. Butler, J. J. Spates, M. A. Mitchell, and W. K. Schubert, *J. Appl. Phys.* **83**:4589 (1998).

15. P. Enoksson, G. Stemme, and E. Stemme, *Sens. Actuators A* **46–47**:327 (1995).

16. T. Corman, P. Enoksson, K. Norén, and G. Stemme, *Meas. Sci. Technol.* **11**:205 (2000).

17. Y. Zhang, S. Tadigadapa, and N. Najafi, *Transducers '01 Eurosensors XV, Proc. 11th Int. Conf. on Solid-State Sensors and Actuators*. (Munich, Germany, 2001).

18. G. Binning, C. F. Quate, and C. Gerber, *Phys. Rev. Lett.* **56**:930 (1986).

19. S. Weigert, M. Dreier, and M. Hegner, *Appl. Phys. Lett.* **69**:2834 (1996).

20. P. I. Oden, G. Y. Chen, R. A. Steele, R. J. Warmack, and T. Thundat, *Appl. Phys. Lett.* **68**:3814 (1996).

21. S. Kirstein, M. Mertesdorf, and M. Schönhoff, *J. Appl. Phys.* **84**:1782 (1998).

22. R. Patois, P. Vairac, and B. Cretin, *Appl. Phys. Lett.* **75**:295 (1999).

23. C. Bergaud and L. Nicu, *Rev. Sci. Instrum.* **71**:2487 (2000).

24. R. Patois, P. Vairac, and B. Cretin, *Rev Sci. Instrum.* **71**:3860 (2000).

25. S. Boskovic, J. W. M. Chon, P. Mulvaney, and J. E. Sader, *J. Rheol.* **46**:891 (2002).

26. N. Ahmed, D. F. Nino, and V. T. Moy, *Rev Sci. Instrum.* **72**:2731 (2001).

27. A. Vidic, D. Then, and Ch. Ziegler, *Ultramicroscopy* **97**:407 (2003).

28. A. Maali, C. Hurth, R. Boisgard, C. Jai, T. Cohen-Bouhacina, and J.-P. Aimé, *J. Appl. Phys.* **97**:074907–1 (2005).
29. D. A. Walters, J. P. Cleveland, N. H. Thomson, P. K. Hansma, M. A. Wendman, G. Gurley, and V. Elings, *Rev. Sci. Instrum.* **67**:3583 (1996).
30. E. Donzier, O. Lefort, S. Spirkovitch, and F. Baillieu, *Sens. Actuators A* **25–27**:357 (1991).
31. R. Lundstrum, A. R. H. Goodwin, K. Hsu, M. Frels, D. Caudwell, J. P. M. Trusler, and K. N. Marsh, *J. Chem. Eng. Data* **50**:1377 (2005).
32. T. Sopkow, K. Hsu, and A. R. H. Goodwin, *J. Chem. Eng. Data* **50**:1732 (2005).
33. C. V. Jakeways and A. R. H. Goodwin, *J. Chem. Thermodyn.* **37**:1093 (2005).
34. A. R. H. Goodwin, E. P. Donzier, O. Vancauwenberghe, M. Manrique de Lara, F. Marty, B. Mercier, A. D. Fitt, K. A. Ronaldson, and W. A. Wakeham, *J. Chem. Eng. Data* **51**:190 (2006).
35. K. A. Ronaldson, A. D. Fitt, A. R. H. Goodwin, and W. A. Wakeham, to *Int. J. Thermophys* (accepted for publication).
36. H. J. McSkimin, *J. Appl. Phys.* **24**:988 (1953).
37. S. P. Nikanorov, S. P. Yu, A. Burenkov, and A. V. Stepanov, *Sov. Phys. Solid State* **13**:2516 (1971).
38. H. Bettin and H. Toth, *Metrologia* **41**:S52 (2004).
39. K. Fujii, in *Experimental Thermodynamics, Vol. VI, Measurement of the Thermodynamic Properties of Single Phases*, A. R. H. Goodwin, K. N. Marsh, and W. A. Wakeham, eds. (Elsevier for International Union of Pure and Applied Chemistry, Amsterdam, 2003), Chap. 5, pp. 191–208.
40. A. Waseda and K. Fujii, *Meas. Sci. Technol.* **12**:2039 (2001).
41. A. Waseda and K. Fujii, *Metrologia* **41**:S62 (2004).
42. C. A. Swenson, *J. Phys. Chem. Ref. Data* **12**:179 (1983).
43. H. J. McSkimin and P. Andreatch Jr., *J. Appl. Phys.* **35**:2161 (1964).
44. H. J. McSkimin and P. Andreatch Jr., *J. Appl. Phys.* **35**:3312 (1964).
45. K. Ronaldson, *Mathematical Modeling of MEMS Densimeters and Viscometers* (Ph.D. Thesis, University of Southampton, United Kingdom, 2006).
46. M. Manrique de Lara and C. Atkinson, *Sensors 2004, Proc. IEEE*, Vol. 2 (2004), pp. 828–831.
47. M. Manrique de Lara, *Development of an Integrated Model of Vibrating Element Fluid Property Sensor* (Ph.D. Thesis, University of London, 2005).
48. T. Bourouina, S. Spirkovitch, F. Marty, F. Baillieu, and E. Donzier, *Appl. Surf. Sci.* **65–66**:536 (1993).
49. G. T. A. Kovacs, N. L. Maluf, and K. E. Petersen, *Proc. IEEE* **86**:1536 (1998).
50. J. B. Mehl, *J. Acoust. Soc. Am.* **64**:1523 (1978).
51. C. Harrison, E. Travernier, O. Vancauwenberghe, E. Donzier, K. Hsu, A. R. H. Goodwin, F. Marty, and B. Mercier, *Sens. Act. A* (in press).
52. Ch. Tegeler, R. Span, and W. Wagner, *J. Phys. Chem. Ref. Data* **28**:779 (1999).
53. E. W. Lemmon and R. T Jacobsen, *Int. J. Thermophys.* **25**:21 (2004).
54. E. W. Lemmon, M. O. McLinden, and M. L. Huber, *Reference Fluid Properties Program (REFPROP) 23, Version 7.1* (Physical and Chemical Properties Division National Institute of Standards and Technology, Boulder, Colorado, 2005).
55. M. J. Assael, H. M. T. Avelino, N. K. Dalaouti, J. M. N. A. Fareleira, and K. R. Harris, *Int. J. Thermophys.* **22**:789 (2001).
56. F. R. Blom, S. Bouwstra, M. Elwenspoek, and J. H. J. Fluitman, *J. Vac. Sci. Technol. B.* **10**:19 (1992).
57. K. Y. Yasumura, T. D. Stowe, E. M. Chow, T. Pfafman, T. W. Kenny, B. C. Stipe, and D. Rugar, *J. Microelectromechanical Syst.* **9**:117 (2000)

58. P. Bruschi, A. Nannini, and F. Pieri, *Sens. Actuators A* **114**:21 (2004)
59. G. C. Maitland, M. Rigby, E. B. Smith, and W. A. Wakeham, *Intermolecular Forces: Their Origin and Determination* (Oxford University Press, Oxford, 1987), p. 571.